



Communication

# Relocking and Locking Range Extension of Partially Locked AMLL Cavity Modes with Two Detuned RF Sinusoids

Shree Krishnamoorthy <sup>1,2,\*</sup>  and Anil Prabhakar <sup>1</sup> <sup>1</sup> Indian Institute of Technology Madras, Chennai 600036, India; anilpr@iitm.ac.in<sup>2</sup> National Center for Biological Sciences, Bengaluru 560065, India

\* Correspondence: shree.krishnamoorthy@tyndall.ie

† Current address: Tyndall National Institute, T12 R5CP Cork, Ireland.

**Abstract:** Actively mode-locked fiber ring lasers (AMLLs) with loss modulators are used to generate approximately 100 ps pulses with 100 MHz repetition. RF detuning around the fundamental frequency,  $f_0$ , causes a loss in phase lock (unlocking) of cavity modes and partial mode locking. Multiple RF inputs are shown, theoretically, to relock and extend the locking range of cavity modes in a detuned partially mode-locked AMLL. A custom-built Yb<sup>3+</sup>-doped AMLL with  $f_0 = 26$  MHz, and operating wavelength of 1064 nm, was used to experimentally verify the theoretical predictions. Two RF sinusoidal signals with constant phase and equal amplitude resulted in an extension of the range by  $X_n = 6.4$  kHz in addition to the range  $R_n = 14.34$  kHz with single input for the mode  $n = 10$ . An increase in locking range was also observed for higher modes. Pulswidth reduction to approximately 205 ps from about 2 ns was also observed in the AMLL.

**Keywords:** fiber lasers; mode locking; active mode locking; partial mode locking; laser cavity resonators; laser mode locking; laser tuning; ring lasers; laser theory; radio frequency; detuned mode locking; mode relocking

## 1. Introduction

Actively mode-locked fiber ring lasers (AMLLs) produce ultrashort pulses with high peak powers and can be synchronized with other light sources for both advanced microscopy and spectroscopic techniques [1–5]. AMLLs have been used to generate both radio frequency (RF) and optical pulsetrains from a laser cavity [6–8]. The versatility of AMLLs for both electrical and ultrashort optical pulses with low maintenance and few stability issues makes them a good candidate for adoption into large systems as synchronized, pulsed multiple laser sources.

Traditionally, pulse formation in an AMLL occurs through the process of mode locking, where all cavity modes, around the central carrier wavelength, are phase-locked with the RF driving signal, typically a single sinusoid. Upon detuning of the driving signal, either due to drift in RF signal or environmental fluctuations, partial locking of the AMLL occurs. This leads to a broadening of pulses due to lock loss of higher modes in both fundamentally and harmonically mode-locked lasers [9–15]. When subject to a large detuning, the laser operates in either Q-switched or amplitude-modulated regimes with pulsewidths in the order of a few ns. This regime also has a wide range of applications, including pulse generation in Raman lasers [12,16–19]. The current methods used to counter detuning are by either modifying the AMLL cavity or using additional optical components. Both of these approaches lead to undesirable changes in the quality of pulses from the laser in terms of synchronization with the source, the pulse's optical wavelength and repetition rate [20–24]. For a successful adoption of AMLLs as optical pulsed sources in synchronized systems, we must develop novel methods to counter the effects of detuning.

Multiple optical injection signals have been used in semiconductor lasers, where the system dynamics have been studied through numerical techniques [25–28]. In such systems,



**Citation:** Krishnamoorthy, S.; Prabhakar, A. Relocking and Locking Range Extension of Partially Locked AMLL Cavity Modes with Two Detuned RF Sinusoids. *Photonics* **2023**, *10*, 735. <https://doi.org/10.3390/photonics10070735>

Received: 27 April 2023

Revised: 11 June 2023

Accepted: 14 June 2023

Published: 27 June 2023



**Copyright:** © 2023 by the authors. Licensee MDPI, Basel, Switzerland. This article is an open access article distributed under the terms and conditions of the Creative Commons Attribution (CC BY) license (<https://creativecommons.org/licenses/by/4.0/>).

there is an improvement in the time bandwidth product, optical linewidth and timing jitter in the laser [27]. Further, multiple injection signals have shown the occurrence of typical Adler-type and atypical Arnold-type locking regimes [28,29]. In this article, we extend our previous work [15,30,31], both theoretically and experimentally, to include multiple RF signals. The use of two RF input signals is a novel method of driving a detuned fiber AMLL. We thus demonstrate an improvement in the number of locked modes by the process of *relocking* using this method for the first time in the literature. Further, we provide a novel demonstration of improvement in the pulsewidths of the partially mode-locked laser with two RF input signals without any additional optical components. We demonstrate a new regime of operation for AMLLs, where, temporally, pulse bunches are produced periodically with varying numbers of locked modes in each of the pulses.

### 2. Theory

Consider the AMLL with multiple loss-modulating RF inputs as shown in Figure 1a. The experimental implementation of the AMLL with two inputs is shown in Figure 1b. The pulse,  $P(f)$ , interacts with the modulation signal,  $M(f)$ , to give  $I(f)$  at the modulator. The optical construction includes a pump (980 nm) coupled to the gain fiber (Yb) using a wavelength division multiplexer (WDM), a circulator and a fiber Bragg grating at 1064 nm, and a 50/50 optical coupler leading to the optical output. The two inputs considered for the experiments are shown in Figure 1b. In this model, we consider the optical energy in the cavity circulating with a fundamental round-trip frequency of  $f_r$ . Periodic loss modulation causes injection of energy into the  $n$ th cavity mode at a frequency  $nf_r$ , in phase lock with the input signal [30,32–34]. In an ideal mode-locked cavity with fundamental resonant frequency,  $f_0$ , the cavity modes occur at frequencies  $nf_0$  and we have  $f_r = f_k = f_0$ , where  $f_k$  is the detuned input frequency.

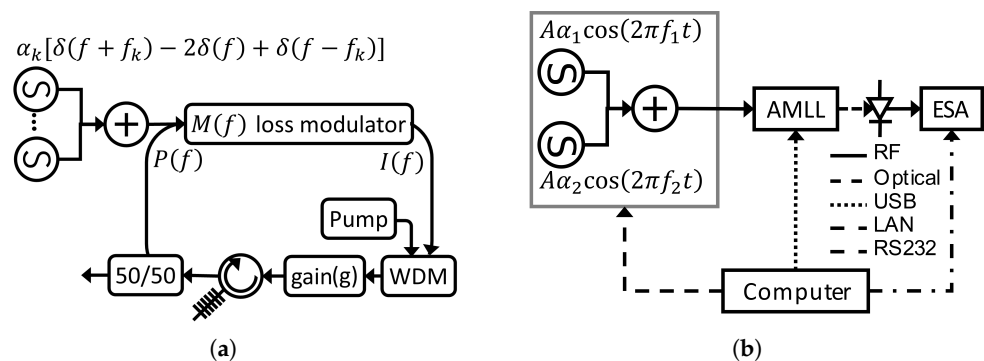


**Figure 1.** (a) AMLL with multiple sinusoids input at the modulator ( $k$ th signal shown). (b) AMLL is fed with two sinusoids from the RF generator for testing the theory. The optical pulses are detected by photodetector and analyzed using the ESA.

In our previous work, for  $f_k = f_0 + \Delta_{0k}$ , where the detuning  $\Delta_{0k} \neq 0$ , we have shown that modes  $n \leq n_{max}$  are locked as they meet the cavity mode’s phase locking conditions, with mode  $n = n_{max}$  forming the edge of the locking range. On the other hand, modes with  $n > n_{max}$  are unlocked, leading to a partially mode-locked and detuned AMLL [30]. In this paper, we show that one can successfully recover the phase lock, i.e., *relock*, an unlocked mode by using multiple sinusoidal inputs at the loss modulator. For this, we extend the single sinusoidal input and single circulating pulse detuned AMLL model to one with multiple sinusoidal inputs and multiple circulating pulses in the cavity.

Consider the total pulse,  $P(f)$ ,

$$P(f) = \sum_r P_r(f) \tag{1}$$

where  $r \in \mathbb{N}$ , and the circulating pulses  $P_r(f)$  have a repetition frequency  $f_r$ , given by,

$$P_r(f) = \gamma_r \sum_n A_n \delta(f - nf_r). \tag{2}$$

$\gamma_r$  is the relative strength such that  $\sum_r \gamma_r = 1$ ,  $A_n$  is the amplitude of the mode  $n$  and  $\delta(\cdot)$  is the Dirac delta function. The detuning of this pulsetrain is  $\Delta_{r0} = f_r - f_0$ .

The AMLL has gain  $g$ , quality factor  $Q$ , central optical frequency  $\nu_s$ , laser linewidth  $\nu_L$  and cold cavity resonance  $f_C$ . Each  $P_r(f)$  individually satisfies the mode locking conditions [35]. Following the treatment from our previous work [30], we describe the perturbed AMLL with multiple inputs and multiple pulsetrains as

$$\sum_r \gamma_r \left\{ j \frac{2Qf_C}{\nu_s f_0} n \Delta_{r0} - g \left[ -2 \frac{n^2 f_0}{\nu_L^2} \Delta_{r0} \right] \right\} A_n = \tilde{I}_n, \tag{3}$$

where  $\tilde{I}_n$  is the modulated amplitude at mode  $n$  and consists of interactions between the pulses and the modulating signal. In this work, we neglect the changes in amplitude  $A_n$  and gain  $g$  in the detuned AMLL. Further, it is assumed that the detuning in the RF signal does not deviate from the central optical frequency  $\nu_s$ . In the next section, we shall look at the perturbed AMLL described in (3) closely.

### 2.1. Interaction of Pulses in the Modulator

As shown in Figure 1a, the total input signal is

$$\mathcal{M}(f) = -M \sum_k \alpha_k [\delta(f + f_k) - 2\delta(f) + \delta(f - f_k)], \tag{4}$$

where the  $k$ th sinusoid has frequency  $f_k$  and the normalized relative amplitude  $\alpha_k$ , such that  $\sum_k \alpha_k = 1$ , and the modulation depth is  $M$ . The total modulating signal,  $I(f)$ , is obtained by convolving (4) with (1):

$$I(f) = -M \sum_k \sum_r \alpha_k [P_r(f + f_k) - 2P_r(f) + P_r(f - f_k)]. \tag{5}$$

Note the injection between adjacent modes due to the action of the sinusoidal modulation. Any pairs of  $f_r$  and  $f_k$  are detuned from each other such that

$$f_k = f_r + \Delta_{kr}. \tag{6}$$

When  $k$  or  $r = 0$ , we refer to the resonant frequency  $f_0$ . We introduce the slow-varying envelope [30,36] to give

$$\tilde{A}_{n\pm 1} = A_{n\pm 1} \exp(j2\pi t(\mp \Delta_{kr})). \tag{7}$$

Using (7) in (5) with (2) and (1), we have

$$I(f) = \sum_n \tilde{I}_{n,\text{Total}} \delta(f - nf_0), \tag{8}$$

where, as shown in Appendix A in (A7),

$$\tilde{I}_{n,\text{Total}} = - \sum_k \sum_r M \alpha_k \gamma_r \left( \tilde{A}_{n+1} - 2A_n + \tilde{A}_{n-1} \right) \exp(j2\pi t n \Delta_{r0}). \tag{9}$$

For each mode  $n$ , we extract the perturbed amplitude as

$$\tilde{I}_n = \tilde{I}_{n,\text{Total}} - I_n, \tag{10}$$

with unperturbed amplitude as

$$I_n = -M(A_{n-1} - 2A_n + A_{n+1}). \tag{11}$$

2.2. Effect on Pulsetrains

To bring out the effect of coupling with multiple inputs, we separate  $\tilde{I}_n$  as

$$\tilde{I}_n = \tilde{I}_{n,R} + \tilde{I}_{n,X}, \tag{12}$$

where  $\tilde{I}_{n,X}$  is generated by coupling between the inputs and  $\tilde{I}_{n,R}$  consists of terms generated by the same input as previously noted [30]

$$\tilde{I}_{n,R} = I_n \sum_r \gamma_r [\exp(j2\pi t n \Delta_{r0}) - 1]. \tag{13}$$

Algebraic simplification for  $\tilde{I}_{n,X}$  (see (A8)–(A12) in Appendix B) gives

$$\tilde{I}_{n,X} = -j4M \sum_r \sum_{k>r} \Gamma_{nrk} D_{nrk} S_{nrk}. \tag{14}$$

where, for any  $(r, k)$ , we have generalized the definitions of  $\beta$ ,  $\Gamma_n$  and  $\Phi_n$  as

$$\beta_{rk} = \gamma_r \alpha_k = \gamma_k \alpha_r, \tag{15}$$

$$\Phi_{nrk} = \tan^{-1} \left[ \frac{A_{n+1} - A_{n-1}}{A_{n+1} + A_{n-1}} \tan \left( 2\pi t n \frac{\Delta_{rk}}{2} \right) \right], \tag{16}$$

$$\Gamma_{nrk} = \beta_{rk} \sqrt{A_{n+1}^2 + A_{n-1}^2 + 2A_{n-1}A_{n+1} \cos(2\pi t n \Delta_{rk})}, \tag{17}$$

$$D_{nrk} = \sin \left( 2\pi t \frac{\Delta_{rk}}{2} \right) \cos \left( 2\pi t \frac{\Delta_{rk}}{2} + \Phi_{nrk} \right) \tag{18}$$

$$\text{and } S_{nrk} = \exp \left( j2\pi t n \frac{\Delta_{r0} + \Delta_{k0}}{2} \right) \tag{19}$$

From (7), we note that, when  $r = k$ ,  $\tilde{I}_{n,X} = 0$ .

2.3. Phase Locking Condition and Locking Limits

Now, we look at the limits to injection locking for the phase condition found from the imaginary parts of Equations (3) and (12)

$$\sum_r \gamma_r \frac{2Qf_c}{v_s f_0} n \Delta_{r0} A_n = I_n \sum_r \gamma_r \sin(2\pi t n \Delta_{r0}) - 4M \sum_r \sum_{k>r} \Gamma_{nrk} D_{nrk} \text{Re}(S_{nrk}). \tag{20}$$

Let us understand qualitatively some of the effects in the phase relationship being captured by the terms in (20). The frequencies  $n\Delta_{r0}$ ,  $n\Delta_{k0}$  and  $n \frac{\Delta_{r0} + \Delta_{k0}}{2}$ , which appear in the terms  $\Gamma_{nrk}$  and  $\frac{\Delta_{rk}}{2}$ , have similar magnitudes. These frequencies are  $n$  times the beat frequency,  $\frac{\Delta_{rk}}{2}$ . When either the  $\sin()$  or  $\cos()$  terms go to zero in (20), the coupling has no influence on the injection range, leading to a time-varying phase locking relationship repeating with the beat frequency in time domain.

For injection locking between all frequencies  $r$ , the maximum frequencies  $\Delta_{r0,max}$  such that all the modes are still locked are possible when all the sinusoidal terms in (20) have unity magnitude to maximize the LHS; i.e.,

$$\sum_r \gamma_r \frac{2Qf_c}{v_s f_0} n \Delta_{r0,max} A_n = I_n + 4M \sum_r \sum_{k>r} \Gamma_{nrk}. \tag{21}$$

Retaining only the frequency terms in the LHS of (21), we obtain the combined maximum locking frequency for all the inputs as

$$\sum_r \gamma_r \Delta_{r0,\max} = \frac{v_s f_0}{2Qf_C} \left( \frac{I_n}{A_n} \frac{1}{n} + \frac{4M \sum_r \sum_{k>r} \Gamma_{nrk}}{A_n} \frac{1}{n} \right). \tag{22}$$

Next, we look at the special case for two inputs where  $r = \{1, 2\}$  with  $\Gamma_n = \Gamma_{n12}$  in (22)

$$\sum_{r=\{1,2\}} \gamma_r \Delta_{r0,\max} = \underbrace{\left( \frac{v_s f_0}{2Qf_C} \frac{I_n}{A_n} \right) \frac{1}{n}}_{\frac{R_n}{2}} + \underbrace{\left( \frac{v_s f_0}{2Qf_C} \frac{4M\Gamma_n}{A_n} \right) \frac{1}{n}}_{\frac{X_n}{2}}. \tag{23}$$

For two inputs, we have only one cross term evident. The first term in the RHS of (23) is the same as for perturbed AMLL applicable for single input given by  $R_n = \frac{v_s f_0}{Qf_C} \left( \frac{I_n}{nA_n} \right)$  [30]. The increase in the total injection range is due to the second term in the RHS, which arises due to coupling between the modes given by

$$X_n = \frac{v_s f_0}{Qf_C} \left( \frac{4M\Gamma_n}{nA_n} \right). \tag{24}$$

For the two RF input cases, we obtain the total range by combining  $R_n$  with (24),  $R_n + X_n$ . We can therefore see that we can recover lock loss beyond the range  $R_n$  by using additional signals. To the author’s knowledge, we are the first to demonstrate an increase in the effective locking range of laser modes without altering the physical parameters of the cavity. This extension of the effective locking range is as shown in (23).

### 3. Experiments and Results

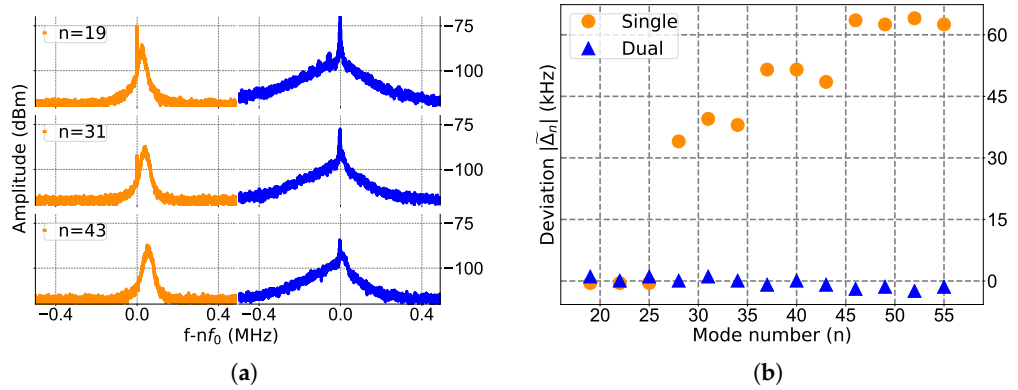
An experiment with two sinusoidal inputs was set up to recover lock loss in higher modes as shown in Figure 1b. A function generator (AFG3252, Tektronix) was used to generate two RF inputs with constant phase relationship at frequencies  $f_1 = f_0 + \Delta_{10}$  and  $f_2 = f_0 + \Delta_{20}$ . The inputs had detuning  $\Delta_{10}$  and  $\Delta_{20}$  from  $f_0 = 26.69$  MHz, which were varied between  $0 \pm 13$  kHz with 90 steps of size 289 Hz each. The two signals were added before feeding to the electro-optic modulator (EOM) of the AMLL. The AMLL construction is already described in our previous work and shown in Figure 1a [30,31]. The optical output of the laser was detected using a fast photodetector with 10 GHz bandwidth (DSC-R402AC, Discovery Semiconductors) and fed to an electrical spectrum analyzer (ESA). The spectrum was collected for each mode  $n$  around  $nf_0$ , with a resolution bandwidth of 500 Hz and span of 2 MHz. The peak amplitude ( $A_n$ ) and frequency of the peak ( $\tilde{f}_n$ ) were recorded for each mode. The complete operation was automated using VISA standards in Python 2.7.

Figure 2 shows the spectra for modes  $n = 19$  to 55, with and without a second input. In Figure 2a-left, only one input is present with  $\Delta_{10} = -0.87$  kHz,  $A = 4$  V-pp and  $\alpha_1 = 1$ . We can see a broad bell-shaped noise spectrum for the modes  $n > 25$  without a distinguishable peak, indicating that they are unlocked. In Figure 2a-right, a second input signal with  $\Delta_{20} = 1.16$  kHz,  $\alpha_1 = 0.5$ ,  $\alpha_2 = 0.5$  and  $A = 4$  V-pp is added. Here, we see distinct peaks in the spectrum for modes  $n > 25$ , indicating relocking in the presence of the second input. To quantify the relocking effect of the second input, we measure the deviation  $|\tilde{\Delta}_n|$  as the difference between the expected peak frequency and the measured peak frequency, given by

$$\tilde{\Delta}_n = \tilde{f}_n - n(\alpha_1 f_1 + \alpha_2 f_2). \tag{25}$$

The deviation shown in Figure 2b indicates a lock loss in mode  $n$  when  $|\tilde{\Delta}_n| > 0$ . For a single input, the modes  $n > 25$  show unlocking. For  $n = \{25 - 55\}$ ,  $|\tilde{\Delta}_n| \approx 0$  when

the second signal is introduced, indicating a relocking of these modes. As a consequence of relocking, a gain of 14 dB is observed in the amplitude of the modes. We have thus demonstrated relocking of the cavity modes of an AMLL by use of two sinusoidal signals at the input and without altering the cavity’s physical properties.



**Figure 2.** Comparison of two cases: single input with  $\Delta_{10} = -0.87$  kHz (orange) and two inputs with  $\Delta_{10} = -0.87$ ,  $\Delta_{20} = 1.16$  kHz (blue). (a) Spectra for modes  $n = 19, 31$  and  $43$ . (b) Mode-wise deviation for modes  $n = 19$  to  $55$ .

Next, to find the limits on relocking frequencies detunings<sub>z</sub> ( $\Delta_{10}$  and  $\Delta_{20}$ ) were varied by up to  $\pm 13$  kHz with step size  $df = 289$  Hz, and deviation  $\tilde{\Delta}_n$  was recorded for modes  $n = \{10, 30, 70\}$ . Figure 3a shows the values of  $|\tilde{\Delta}_n|$  for mode  $n = 10$ . The white dots mark the edges of the locked regions such that  $\tilde{\Delta}_n < 10$  kHz, evaluated using a Laplacian filter with a threshold  $\mathcal{T}$  set heuristically for a given mode [37]. For  $\Delta_{10}$ , the maximum possible range is  $R_{10} + X_{10}$  of 20.74 kHz within which relocking was successful, with the two inputs marked with dashed lines. The single input case where a range of  $R_{10} = 14.34$  kHz was obtained for the same AMLL is also shown for comparison [30]. There is an increase of 6.4 kHz in the locking range for the 10th mode when two inputs are used. Similarly, an increase in range  $R_n + X_n$  was observed when compared to  $R_n$  for  $n = 30$  and  $70$ , as shown in Figure 3b. To our knowledge, such an expansion of the locking range has been demonstrated in the work presented here for the first time.

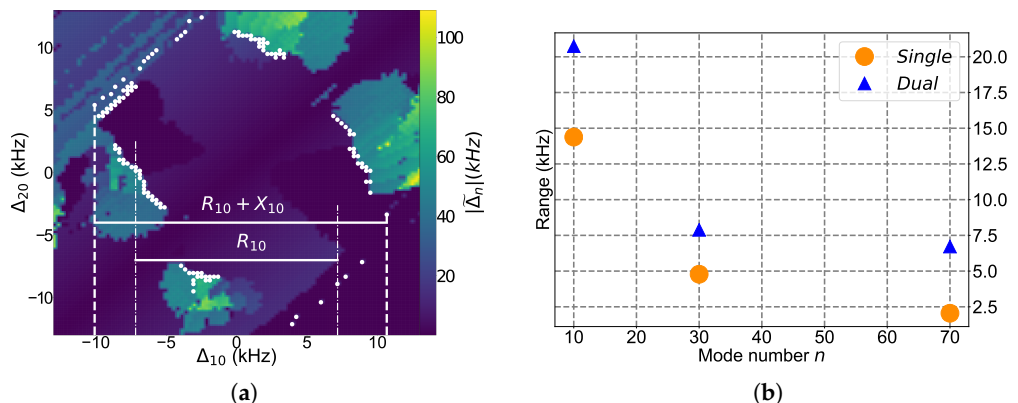


**Figure 3.** (a) Deviation for mode  $n = 10$  with two injection signals ( $\Delta_{10} = -0.87$ ,  $\Delta_{20} = 1.16$  kHz). (b) Injection ranges for modes  $n = 10, 30, 70$  for single- ( $R_n$  in orange) and two-input injection ( $R_n + X_n$  in blue).

To look at the effect of relocking with a second input in the time domain, the time traces (using Textronix MDO3104 oscilloscope) and pulsewidth (using sampling oscilloscope (Lecroy SDA 100G)) after the fast photodetector were recorded. Figure 4 shows the

pulsewidth (full-width half-maximum) for an average of 16 pulses triggered above the noise level. Figure 4a shows the pulsewidths for varying  $\Delta_{10}$  and with and without the second input. For single input, the pulsewidth increases as  $|\Delta_{10}|$  increases. Upon addition of a second input, one can observe a decrease in pulsewidth from approximately  $\sim 2$  ns to  $\sim 205$  ps, where the reduced pulsewidth matches the mode-locked AMLL pulsewidth for a single input with  $\Delta_{10} = 0$  kHz. Figure 4b shows the averaged pulse traces corresponding to points (i)–(iv) in Figure 4a, where  $\Delta_{10} = -7, -2, -0.8$  and approximately 0 kHz, respectively. With two inputs, one can observe the reduced pulsewidth with a second RF input with  $\Delta_{20} = 279, 359, 277$  and 211 kHz corresponding to  $\Delta_{10} = -7, -2, -0.8$  and about 0 kHz, respectively. A reduction in pulsewidth is clearly visible. Note that pedestals in the traces could arise due to the averaging of pulse traces with a distribution of pulse shapes and widths between them, as predicted regarding the time-varying nature of the phase locking condition between the pulses in the pulse bunches (20). We believe that this is the first demonstration of a reduction in pulsewidth to mode-locked widths via relocking of higher modes with the use of two signals at the RF input in a fiber AMLL.

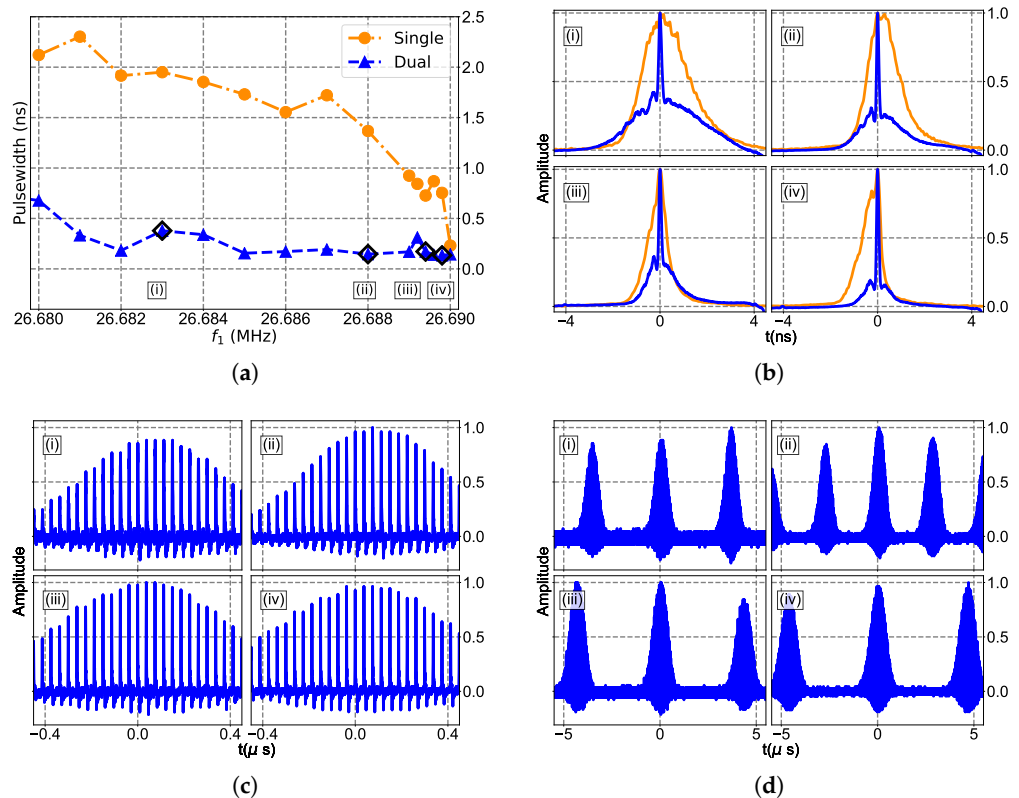


**Figure 4.** (a) Pulsewidth for different  $f_1$  in the presence (blue) and absence (orange) of a second input. The points (i)–(iv) are taken as examples to demonstrate the effect a second input has on the pulses. (b) Pulses at points (i)–(iv) in (a) for single (orange) and two (blue) inputs. (c)  $\approx 25$  pulses in the pulsetrain for two inputs for cases (i)–(iv). (d) Pulsetrains for 11  $\mu\text{s}$  for two inputs for cases (i)–(iv).

Figure 4c,d shows pulsetrains corresponding to the points (i)–(iv) with two inputs. Varying quality in pulses for about 25 pulses in each case is shown in Figure 4c. In Figure 4d, we have the pulsetrain for 11  $\mu\text{s}$  for two inputs. We observe the occurrence of pulse bunches, consisting of many pulses separated by time periods of 3.77, 2.8 and 4.73  $\mu\text{s}$  corresponding to points (i), (ii) and (iv) with the corresponding  $\Delta_{10} + \Delta_{20} = 265, 355$  and 211 kHz. This is in agreement with the theory presented in the previous section, where the slower time-varying nature in the phase condition is contained in the term  $D_{nrk}$  in (20). However, for point (iii), with  $\Delta_{10} + \Delta_{20} = 275.2$  kHz, the bunches themselves have a larger time period between them, which could be due to different operating regimes of operations and other non-linearities in the cavity.

#### 4. Conclusions

In this paper, multiple RF input signals in an AMLL are shown as a novel method to extend the locking range of the cavity modes. We observe an increase in the number of locked modes and reduction in pulsewidths. A time-varying frequency model developed in this paper predicts locking of unlocked modes in a partially mode-locked laser when a second RF signal is used. The non-stationary model developed here also predicts the time-varying nature of the locking dynamics in the laser output with two inputs. Experimentally, it is demonstrated here that two sinusoidal RF inputs extend the locking range for 10th mode from  $R_{10} = 14.34$  kHz by  $X_{10} = 6$  kHz. The increased number of locked modes causes a narrowing of pulses in a partially locked laser from 2 ns to 205 ps.

**Author Contributions:** Conceptualization, S.K.; methodology, S.K.; software, S.K.; validation, S.K.; formal analysis, S.K.; investigation, S.K.; resources, A.P.; data curation, S.K.; writing—original draft preparation, S.K.; writing—review and editing, S.K. and A.P.; visualization, S.K.; supervision, A.P.; project administration, A.P.; funding acquisition, S.K. and A.P. All authors have read and agreed to the published version of the manuscript.

**Funding:** S. Krishnamoorthy thanks BERI for supporting her research and providing the opportunity to be associated with the project. She also thanks IPIC, Science Foundation Ireland (SFI) (Grant ID SFI/15/RP/2828 and SFI/22/RP-2TF/10293) and Tyndall National Institutes for providing sustenance during the manuscript preparation.

**Institutional Review Board Statement:** Not applicable.

**Informed Consent Statement:** Not applicable.

**Data Availability Statement:** Data underlying the results presented in this paper are not publicly available at this time but may be obtained from the authors upon reasonable request.

**Acknowledgments:** The authors thank Jayavel D., Yusuf Panbiharwala and Sathish for help with construction of the lasers. The authors thank Satyajit Mayor and Central Imaging & Flow Cytometry Facility (CIFF) at NCBS-TIFR, Bangalore, as well as the photonics@IITM group and Jitu lab for facilities, and Stefan Andersson-Engles, Julie Donnelly, Simon Sorensen, Baptiste Jayet, Benjamin Lingnau, Michael Dillane, BioPhotonics@Tyndall, Aravind P. Anthur and Deepa Venkatesh for useful suggestions. The authors wish to thank the anonymous reviewers for their valuable suggestions.

**Conflicts of Interest:** The authors declare no conflict of interest.

#### Appendix A. Derivation of $\tilde{I}_n$

To observe the impact of this interaction on individual cavity mode, we recognize that each pulsetrain,  $P_r(f)$ , is composed of the contribution from each cavity mode  $n$  with amplitude  $A_n$  at frequency  $nf_r$ , such that one can write

$$P_r(f) = \gamma_r \sum_n A_n \delta(f - nf_r) \tag{A1}$$

where  $\gamma_r$  is the relative strength of the pulsetrain having repetition rate  $f_r$  such that  $\sum_r \gamma_r = 1$ . The total pulse in (1) can be expressed as

$$P(f) = \sum_{r \in \mathbb{N}} \gamma_r \sum_n A_n \delta(f - nf_r) \tag{A2}$$

Using (5) and (A2), we have

$$I(f) = - \sum_{k \in \mathbb{N}} M\alpha_k \sum_{r \in \mathbb{N}} \gamma_r \left[ \sum_n A_n \delta(f - nf_r + f_k) - 2 \sum_n A_n \delta(f - nf_r) + \sum_n A_n \delta(f - nf_r - f_k) \right]. \tag{A3}$$

To evaluate the effect of perturbation in the system described above, we note with indices  $k, r \in \mathbb{N}$ , the frequencies  $f_r$  and  $f_k$  are both detuned from  $f_0$  such that  $f_{(k \text{ or } r)} = f_0 + \Delta_{(k \text{ or } r)}$  and  $f_k = f_r + \Delta_{kr}$ .



Using (A3) and regrouping the terms under a common summation in  $n$ , we have

$$I(f) = -M \sum_{k \in \mathbb{N}} \alpha_k \sum_{r \in \mathbb{N}} \gamma_r \sum_n \left( \tilde{A}_{n+1} - 2A_n + \tilde{A}_{n-1} \right) \delta(f - nf_r). \tag{A4}$$

Note that the effects of amplitude and phase change from the coupling are absorbed in the terms  $\tilde{A}_{n+1}$  and  $\tilde{A}_{n-1}$ . Now, we can represent the total modulated amplitude,  $I(f)$  in (A4), as a sum of  $\tilde{I}_{n,\text{Total}}$  for each mode  $n$  as

$$I(f) = \sum_n \tilde{I}_{n,\text{Total}} \delta(f - nf_0), \tag{A5}$$

where we have the perturbed amplitude

$$\tilde{I}_n = \tilde{I}_{n,\text{Total}} - I_n, \tag{A6}$$

with  $I_n$  given by (11) and

$$\tilde{I}_{n,\text{Total}} = - \sum_{k \in \mathbb{N}} \sum_{r \in \mathbb{N}} M \alpha_k \gamma_r \exp(j2\pi t n \Delta_{r0}) \left( \tilde{A}_{n+1} - 2A_n + \tilde{A}_{n-1} \right). \tag{A7}$$

### Appendix B. Two Input $\tilde{I}_{n,X}$

To simplify the expression for the cross terms, we first look at a case with only two inputs. For two inputs, we expand  $\tilde{I}_{n,X}$  for  $r = \{1, 2\}$  and  $k = \{1, 2\}$  as

$$\tilde{I}_{n,X} \triangleq -M2j \sin\left(2\pi t \frac{\Delta_{12}}{2}\right) \exp\left(j2\pi t n \frac{(\Delta_{10} + \Delta_{20})}{2}\right) \left[ \exp\left(j2\pi t \frac{\Delta_{12}}{2}\right) \Gamma_n \exp(j\Phi_n) + \exp\left(-j2\pi t \frac{\Delta_{12}}{2}\right) \Gamma_n \exp(-j\Phi_n) \right]. \tag{A8}$$

where we have noted that  $\Delta_{12} = -\Delta_{21}$  and,

$$\Gamma_n \exp(j\Phi_n) = \gamma_1 \alpha_2 \exp\left(j2\pi t n \frac{\Delta_{12}}{2}\right) A_{n+1} + \gamma_2 \alpha_1 \exp\left(-j2\pi t n \frac{\Delta_{12}}{2}\right) A_{n-1}. \tag{A9}$$

Further, we note that the magnitude term  $\Gamma_n$  is real and positive,  $0 \leq \alpha_1, \alpha_2 \leq 1$  and  $0 \leq \gamma_1, \gamma_2 \leq 1$ , which leads to the condition for cross terms as

$$\beta = \gamma_1 \alpha_2 = \gamma_2 \alpha_1. \tag{A10}$$

Using (A10) with (A9), we have

$$\Gamma_n = \beta \sqrt{\left( A_{n+1}^2 + A_{n-1}^2 + 2A_{n-1}A_{n+1} \cos\left(2\pi t n \Delta_{12}\right) \right)}. \tag{A11}$$

Next, from (A9) and (A10), we obtain the value for  $\Phi_n$  as

$$\Phi_n = \tan^{-1} \left[ \frac{A_{n+1} - A_{n-1}}{A_{n+1} + A_{n-1}} \tan\left(2\pi t n \frac{\Delta_{12}}{2}\right) \right] \tag{A12}$$

### References

1. Cicerone, M.T.; Camp, C.H. Histological coherent Raman imaging: A prognostic review. *Analyst* **2018**, *143*, 33–59. [[CrossRef](#)]
2. Yang, B.; Fang, C.-Y.; Chang, H.-C.; Treussart, F.; Trebbia, J.-B.; Lounis, B. Polarization effects in lattice-*STED* microscopy. *Faraday Discuss.* **2015**, *184*, 37–49. [[CrossRef](#)] [[PubMed](#)]
3. Klar, T.A.; Jakobs, S.; Dyba, M.; Egner, A.; Hell, S.W. Fluorescence microscopy with diffraction resolution barrier broken by stimulated emission. *Proc. Natl. Acad. Sci. USA* **2000**, *97*, 8206–8210. [[CrossRef](#)] [[PubMed](#)]

4. Takasaki, K.T.; Ding, J.B.; Sabatini, B.L. Live-cell superresolution imaging by pulsed STED two-photon excitation microscopy. *Biophys. J.* **2013**, *104*, 770–777. [[CrossRef](#)] [[PubMed](#)]
5. Sidenstein, S.C.; D'Este, E.; Böhm, M.J.; Danzl, J.G.; Belov, V.N.; Hell, S.W. Multicolour multilevel STED nanoscopy of actin/spectrin organization at synapses. *Sci. Rep.* **2016**, *6*, 26725. [[CrossRef](#)]
6. Yao, X.S.; Davis, L.; Maleki, L. Coupled optoelectronic oscillators for generating both RF signal and optical pulses. *J. Light. Technol.* **2000**, *18*, 73–78. [[CrossRef](#)]
7. Yin, K.; Zhang, B.; Yang, W.; Chen, H.; Chen, S.; Hou, J. Flexible picosecond thulium-doped fiber laser using the active mode-locking technique. *Opt. Lett.* **2014**, *39*, 4259–4262. [[CrossRef](#)]
8. Xiao, K.; Jin, X.; Jin, X.; Yu, X.; Zhang, X.; Zheng, S.; Chi, H.; Feng, L.; Xu, M. Channelized amplification of RF signal based on actively mode locked fiber laser. *Opt. Commun.* **2018**, *421*, 46–49. [[CrossRef](#)]
9. Hjelm, D.R.; Mickelson, A.R. Theory of timing jitter in actively mode-locked lasers. *IEEE J. Quantum Electron.* **1992**, *28*, 1594–1606. [[CrossRef](#)]
10. Eichler, H.J.; Koltchanov, I.G.; Liu, B. Numerical study of the spiking instability caused by modulation frequency detuning in an actively mode-locked solid-state laser. *Appl. Phys. B* **1995**, *61*, 81–88. [[CrossRef](#)]
11. Wu, S.-Y.; Hsiang, W.-W.; Lai, Y. Synchronous-asynchronous laser mode-locking transition. *Phys. Rev. A* **2015**, *92*, 013848. [[CrossRef](#)]
12. Lee, J.; Lee, J.H. Experimental investigation of the cavity modulation frequency detuning effect in an active harmonically mode-locked fiber laser. *J. Opt. Soc. B Am. Opt. Phys.* **2013**, *30*, 1479–1485. [[CrossRef](#)]
13. Krishnamoorthy, S.; Mayor, S.; Prabhakar, A. Synchronization between two fixed cavity mode locked lasers. In Proceedings of the 5th International Conference on Photonics, Optics and Laser Technology, Porto, Portugal, 27 February–1 March 2017; Volume 1, pp. 273–282.
14. Krishnamoorthy, S.; Thiruthakkathevan, S.; Prabhakar, A. Active fibre mode-locked lasers in synchronization for STED microscopy. In *Optics, Photonics and Laser Technology 2017*; Springer: Berlin/Heidelberg, Germany, 2019; pp. 233–253.
15. Krishnamoorthy, S. Mode Unlocking and Relocking in a Detuned Actively Mode Locked Fiber Ring Laser. Ph.D. Thesis, Indian Institute of Technology Madras, Chennai, India, 2020.
16. Kuznetsov, A.; Kharenko, D.; Podivilov, E.; Babin, S. Fifty-ps raman fiber laser with hybrid active-passive mode locking. *Opt. Express* **2016**, *24*, 16280–16285. [[CrossRef](#)] [[PubMed](#)]
17. Kuznetsov, A.G.; Kablukov, S.I.; Timirtdinov, Y.A.; Babin, S.A. Actively mode locked raman fiber laser with multimode ld pumping. *Photonics* **2022**, *9*, 539. [[CrossRef](#)]
18. Yang, X.; Zhang, L.; Jiang, H.; Fan, T.; Feng, Y. Actively mode-locked raman fiber laser. *Opt. Express* **2015**, *23*, 19831–19836. [[CrossRef](#)]
19. Koliada, N.A.; Nyushkov, B.N.; Ivanenko, A.V.; Kobtsev, S.M.; Harper, P.; Turitsyn, S.K.; Denisov, V.I.; Pivtsov, V.S. Generation of dissipative solitons in an actively mode-locked ultralong fibre laser. *Quantum Electron.* **2013**, *43*, 5. [[CrossRef](#)]
20. Yao, J.; Yao, J.; Wang, Y.; Tjin, S.C.; Zhou, Y.; Lam, Y.L.; Liu, J.; Lu, C. Active mode locking of tunable multi-wavelength fiber ring laser. *Opt. Commun.* **2001**, *191*, 341–345. [[CrossRef](#)]
21. Lee, C.G.; Kim, Y.J.; Park, C.-S. Optical pulse shaping by cross-phase modulation in a harmonic mode-locked semiconductor fiber ring laser under large cavity detuning. *J. Light. Technol.* **2006**, *24*, 1237.
22. Nakazawa, M.; Yoshida, E. A 40 GHz 850 fs regeneratively FM mode-locked polarization-maintaining erbium fiber ring laser. *IEEE Photonics Technol. Lett.* **2000**, *12*, 1613–1615. [[CrossRef](#)]
23. Wise, F.; Lefrançois, S. Fiber Source of Synchronized Picosecond Pulses for Coherent Raman Microscopy and Other Applications. U.S. Patent 10,608,400, 31 March 2020.
24. Sato, K.; Ishii, H.; Kotaka, I.; Kondo, Y.; Yamamoto, M. Frequency range extension of actively mode-locked lasers integrated with electroabsorption modulators using chirped gratings. *IEEE J. Sel. Top. Quantum Electron.* **1997**, *3*, 250–255. [[CrossRef](#)]
25. York, R.A. Nonlinear analysis of phase relationships in quasi-optical oscillator arrays. *IEEE Trans. Microw. Theory Techn.* **1993**, *41*, 1799–1809. [[CrossRef](#)]
26. Yeung, M.S.; Strogatz, S.H. Time delay in the Kuramoto model of coupled oscillators. *Phys. Rev. Lett.* **1999**, *82*, 648. [[CrossRef](#)]
27. Habruseva, T.; Huyet, G.; Hegarty, S.P. Dynamics of quantum-dot mode-locked lasers with optical injection. *IEEE J. Sel. Top. Quantum Electron.* **2011**, *17*, 1272–1279. [[CrossRef](#)]
28. Shortiss, K.; Lingnau, B.; Dubois, F.; Kelleher, B.; Peters, F.H. Harmonic frequency locking and tuning of comb frequency spacing through optical injection. *Opt. Express* **2019**, *27*, 36976–36989. [[CrossRef](#)] [[PubMed](#)]
29. Lingnau, B.; Shortiss, K.; Dubois, F.; Peters, F.H.; Kelleher, B. Universal generation of devil's staircases near hopf bifurcations via modulated forcing of nonlinear systems. *Phys. Rev. E* **2020**, *102*, 030201. [[CrossRef](#)]
30. Krishnamoorthy, S.; Prabhakar, A. Mode unlocking characteristics of an RF detuned actively mode-locked fiber ring laser. *Opt. Commun.* **2019**, *431*, 39–44. [[CrossRef](#)]
31. Krishnamoorthy, S.; Mayor, S.; Prabhakar, A. Mode re-locking in an RF detuned actively mode-locked fiber ring laser. In Proceedings of the The European Conference on Lasers and Electro-Optics, Munich, Germany, 23–27 June 2019.
32. Adler, R. A study of locking phenomena in oscillators. *Proc. IRE* **1946**, *34*, 351–357. [[CrossRef](#)]
33. Strogatz, S.H. *Nonlinear Dynamics and Chaos: With Applications to Physics, Biology, Chemistry, and Engineering*; Westview Press: Boulder, CO, USA, 2014.

34. Razavi, B. A study of injection pulling and locking in oscillators. In Proceedings of the IEEE 2003 Custom Integrated Circuits Conference, San Jose, CA, USA, 24 September 2003; pp. 305–312.
35. Haus, H.A. A theory of forced mode locking. *IEEE J. Quant. Electron.* **1975**, *11*, 323–330. [[CrossRef](#)]
36. Tse, D.; Viswanath, P. *Fundamentals of Wireless Communication*; Cambridge University Press: Cambridge, UK, 2005.
37. Gonzalez, R.C.; Woods, R.E. *Digital Image Processing*; Pearson-Prentice-Hall Upper Saddle River: Saddle River, NJ, USA, 2002.

**Disclaimer/Publisher’s Note:** The statements, opinions and data contained in all publications are solely those of the individual author(s) and contributor(s) and not of MDPI and/or the editor(s). MDPI and/or the editor(s) disclaim responsibility for any injury to people or property resulting from any ideas, methods, instructions or products referred to in the content.